The myosin filament XIV backbone structure

Francis T. Ashton, John Weisel, and Frank A. Pepe
Department of Anatomy, School of Medicine, University of Pennsylvania, Philadelphia, Pennsylvania 19104-6058 USA

ABSTRACT The substructure of the thick filaments of chemically skinned chicken pectoralis muscle was investigated by electron microscopy. Images of transverse sections of the myosin filaments were determined to have threefold symmetry by cross-correlation analysis, which gives an unbiased determination of the rotational symmetry of the images. Resolution, using the phase residual test (Frank et al. 1981. *Science [Wash. DC]*. 214:1353–1355), was found to be between 3.2 and 3.6 nm. Three arrangements of nine subfilaments in the backbone were found in all regions of the filament at ionic strengths of 20 and 200 mM. In the average images of two of these, there were three dense central subfilaments and three pairs of subfilaments on the surface of the thick filament. In the average image of the third arrangement, all of the protein mass of the nine subfilaments was on the surface of the filament with three of them showing less variation in position than the others. A fourth arrangement appearing to be transitional between two of these was seen often at 200 mM ionic strength and only rarely at 20 mM. On average, the myosin subfilaments were parallel to the long axis of the filament. The different arrangements of subfilaments appear to be randomly distributed among the filaments in a transverse section of the A-band. Relative rotational orientations with respect to the hexagonal filament lattice, using the three densest subfilaments as reference showed a major clustering (32%) of filaments within one 10° spread, a lesser clustering (15%) at 90° to the first, and the remainder scattered thinly over the rest of the 120° range. There was no obvious pattern of distribution of the two predominant orientations that could define a superlattice in the filament lattice.

INTRODUCTION

The structure of vertebrate skeletal myosin filaments has been the subject of much study (Huxley, 1963; Pepe, 1966*a*, *b*, 1967*a*, *b*, Squire, 1973; Stewart et al., 1981). From X-ray diffraction studies (Huxley and Brown, 1967), it is known that myosin cross-bridges occur at intervals of 14 nm in a helical arrangement with an axial repeat of 43 nm. Recently, considerable evidence has been obtained for a three-stranded helical arrangement of the myosin cross bridges on the surface of the myosin filament (Kensler and Stewart, 1983; Ip and Heuser, 1983; Varrano-Marston et al., 1984; Knight et al., 1986; Stewart and Kensler, 1986). In transverse sections of the myosin filament observed by electron microscopy, the presence of subfilaments with a center to center spacing of ~4 nm has been reported (Pepe and Drucker, 1972; Stewart et al., 1981; Pepe et al., 1986). The clearest observation of these subfilaments has been made using a multistage fixation procedure before embedding and sectioning the muscle (Ashton and Pepe, 1981). Subfilament spacings of ~4 nm have also been observed by X-ray diffraction in vertebrate skeletal muscle (Millman, 1979) as well as in the myosin filaments of crustacean muscle (Wray, 1979). Because the α-helical myosin rod has a diameter of ~2 nm, a 4-nm spacing between subfilaments suggests that there is more than one myosin molecule in a transverse section through each subfilament. Myosin filaments can be splayed into three parallel units (Maw and Rowe, 1980; Pepe, 1982) that probably represent another level of structural organization of the filament. Each of these units has a diameter larger than the spacing between subfilaments and would therefore probably be made up of more than one subfilament.

The substructure of vertebrate skeletal myosin filaments determined by applying computer image processing techniques to electron micrographs of transverse sections of myosin filaments consists of nine densities (three central and six peripheral) which are consistently present. This observation led to the conclusion that there are nine subfilaments in the myosin filament. Three other weaker densities are sometimes observed (Pepe and Drucker, 1972; Stewart et al., 1981) and are probably due to the portion of the myosin cross-bridges arising from the central three subfilaments and projecting to the surface of the filament (Pepe et al., 1986). This finding of nine subfilaments is consistent with the evidence for a three-stranded myosin cross-bridge arrangement on the surface of vertebrate skeletal myosin filaments (Kensler and Stewart, 1983; Ip and Heuser, 1983; Varrano-Marston et al., 1984; Knight et al., 1986).

The main purpose of this research is to determine the structure of the backbone of the myosin filaments in more detail, taking special care to assess the validity of each step of the analysis of our findings. We have

0006-3495/92/06/1513/16 $2.00

obtained evidence for (*a*) the presence of threefold symmetry in the backbone structure, (*b*) the resolution obtainable in the average images used, (*c*) the existence of different arrangements of subfilaments, and (*d*) the representation of the different arrangements in different regions of the filament.

MATERIALS AND METHODS

Preparation of skinned fibers and fixation

All of these studies were done with the pectoralis muscles of the adult chicken. Thin muscle strips ~1–2 mm in diameter were dissected out of fresh muscle and pinned with stainless steel pins to soft plastic blocks (Sylgard) under slight tension so that they were taut. The strips were immersed at 0°–4°C overnight in a solution containing 150 mM K proprionate, 5 mM KH_2PO_4, 3 mM Mg acetate, 3 mM adenosine triphosphate (ATP), 5 mM ethyleneglycol-bis(β-aminoethyl ether-*N*-*N*′-tetracetic acid (EGTA), and 1 mM dithiothreitol (DTT), at pH 7.0 (Brenner et al., 1984). Proteolytic inhibitors, E 64 (Hanada et al., 1978) at a concentration of 0.5 mM and phenylmethylsulfonyl fluoride (PMSF) at a concentration of 1 mM were added. After incubation in this solution, bundles consisting of about two to six single muscle fibers were dissected out in fresh solution on ice and pinned to soft plastic blocks (Sylgard) with stainless steel pins. Before pinning the fiber bundles, a groove was cut out of the plastic so that the side of the fiber bundle closest to the plastic was not in contact with the plastic. These bundles were then exposed to the same solution containing 0.5% Triton-X 100 for 20–30 min, and washed with the same solution without Triton-X 100 to remove the detergent. The fibers were then washed with the solution in which they were to be studied, using three washes of about 10 min each, and incubated in the same solution overnight. Three solutions were used in these studies: (*a*) Low ionic strength (20 mM containing 5-adenylylimidodiphosphate [AMP-PNP]), consisting of 1 mM AMPPNP, 1 mM EGTA, 3 mM $MgCl_2$, 1 mM DTT, 10 mM imidazole, pH 7.0 (after Brenner et al., 1984); (*b*) high ionic strength (200 mM, relaxed), consisting of 5.44 mM adenosine triphosphate (ATP), 25 mM EGTA, 7.7 mM $MgCl_2$, 10 mM glutathione, 19.11 mM phosphocreatine, 100 mM *N*-tris(hydroxymethyl)methyl-2-aminoethane sulfonic acid (TES), pH 7.1 (Dantzig and Goldman, 1985); (*c*) high ionic strength (200 mM, rigor), consisting of 51.48 mM EGTA, 3.23 mM $MgCl_2$, 100 mM TES, pH 7.1 (Dantzig and Goldman, 1985). After overnight incubation, the fibers were washed with the same solution, and fixed with 4% glutaraldehyde in the same solution for 4 h. This glutaraldehyde fixation which is the first step of the multistage fixation procedure described previously (Ashton and Pepe, 1981) was followed by overnight washing in the same experimental solution without glutaraldehyde. Then fixation proceeded using the buffer of the published procedure, i.e., 0.1 M cacodylate, 6% sucrose, 0.12 mM $CaCl_2$, pH 7.2, henceforth designated as buffer pH 7.2. The next fixation was for 2 h in 0.1 M 1-cyclohexyl-3 morpholino-ethyl carbodiimide-mentho-*p*-toluene sulfate (CDI), 1.0 M ethylene diamine (EDA) in buffer pH 7.2. After a 15–20-min wash in buffer pH 7.2, the sample was fixed for 2 h with 20 mg/ml dimethyl suberimidate (DMS), 20 mg/ml dimethyl adipimidate (DMA) in the buffer adjusted to pH 8. After a 15–20-min wash in buffer pH 7.2 and then for 2 h in 0.2 M EDA in buffer pH 7.2, the fibers were again washed for 15–20 min in buffer pH 7.2 and then overnight in fresh buffer pH 7.2. The sample was then fixed for 2 h in 4% glutaraldehyde in buffer pH 7.2, washed for 15–20 min in buffer pH 7.2, and finally fixed for 20 min in 1% osmium tetroxide in 0.1 M cacodylate pH 7.2 (i.e., buffer pH 7.2 without sucrose or $CaCl_2$). Fixation was followed by dehydration in acetone and embedding in araldite as previously described (Pepe et al., 1981).

Electron microscopy

Serial transverse sections ~110 nm thick were obtained on a model MT-2 microtome (DuPont-Sorvall, Newtown, CT) using a diamond knife. The position of a section along the length of the filament was determined by following a particular area of the myofibril from section to section in the series and counting the number of sections throughout the entire length of the A-band. From the number of sections and the known 1.6-mm length of the A-band, the thickness of the sections could be confirmed. Counting the number of sections in the series either from the tapered ends of the filaments (edge of the A-band) or from the M-band (middle of the A-band) determined the position of the section along the length of the filament. In all cases filaments were viewed looking from the M-band toward the Z-band. Three regions along the length of the filament were studied, and these were identified using the terminology of Sjostrom and Squire (1977): (*a*) between the bare zone and the C-protein–bearing region (P region), (*b*) in the C-protein–bearing region, (C region), and (*c*) beyond the C-region but not including the tapered ends of the filament (D region). This scheme identifies three approximately equal portions of each half of the myosin filament. Micrographs were taken at magnification of 100,000. The micrographs selected for study were digitized on a model P-1000 Photoscan (Optronics Engineering, Goleta, CA) with pixel size 50 × 50 μm on the electron micrograph, corresponding to 0.5 × 0.5 nm in the specimen.

Image selection criteria

Areas containing ~150–175 myosin filament images in one negative were chosen for study. About 5% of these images were discarded because they were badly disrupted based on visual inspection. About 20% of the remaining images were discarded because they did not have threefold symmetry, and the other 80% of the images were processed as described below.

Image analysis and averaging

Computer image processing was carried out on a VAX750 (Digital Equipment Corp., Marlboro, MA). Programs were written in FORTRAN using conventional Fourier algorithms. Cross-correlation analysis and rotational averaging were used to process the images. For cross-correlation alignment of images, the SPIDER package of software provided by Dr. Joachim Frank was used (Frank et al., 1981*a*). Alignment of the images was done with respect to a reference image taken from the group to be aligned. The reference was chosen for uniformity of density distribution and definition of substructure, and the process was carried out several times with different reference images to check for consistency. The images were first roughly aligned rotationally by cross correlation of the autocorrelation maps of each image with the autocorrelation map of the reference image. The images themselves were then each cross correlated with the reference image itself for both rotational and translational alignment and the aligned images were averaged. This average image was then used as a reference for a second cycle of rotational and translational cross correlation omitting use of the autocorrelation maps. The average of these realigned images was then used as a reference for a third rotational and translational alignment. The center of mass (of pixel density) of the average image obtained in this way was determined so that the image could be rotationally filtered. A map of rotational power versus frequency was plotted to get information about the

symmetry of the average image. The rotational filtering was performed using the general Fourier-Bessel framework laid down by Crowther and Amos (1971), as described previously (Stewart et al., 1981; Pepe et al., 1986). The input images were initially expressed in Cartesian coordinates and were transformed to polar coordinates by bilinear interpolation. Circumferential Fourier transforms were produced at a selected number of radial steps, generally one step per pixel, and a power spectrum was generated showing the frequency components of the image at each radius, as well as the totals over all radii. Individual images were also rotationally filtered. In this case the centers were determined by finding the point in each image where n-fold Fourier power was the highest percentage of total (nonzero order) power. When images were reconstructed this was done using the n-fold harmonics, i.e., for threefold symmetry including frequencies of 3, 6, 9, 12, and 15. Images were observed on an advanced electronics design color graphics terminal and photographed with a color graphics camera from Matrix Instruments (Orangeburg, NY).

Assessing the validity of the results

To emphasize and therefore verify differences between average images, one normalized average image was sometimes subtracted from another. In these cases, the statistical significance of the difference image was determined by applying the criterion that significant differences were those that were greater than three times the standard error of the corresponding pixel density of each of the average images used (Zingsheim et al., 1982). To apply this criterion the density distribution of the images used must be Gaussian. The existence of Gaussian density distributions was established by applying the Kolmogorov-Smirnov goodness of fit test (Sachs, 1984). To assess the validity of an average image, (*a*) the variance and standard deviation of the average image was obtained and (*b*) the images making up the average were split into two independent averages for comparison and the phase residuals were computed (Frank et al., 1981*b*). The phase residuals were calculated for a series of rings from the Fourier transforms of the two images. For each ring the phase residual was calculated first for one image from each group and then repeated each time another image was added to each group. For each ring in the Fourier transform, plots of the phase residual after each addition were made. The resolution was determined by allowing a maximum phase residual of 45° (Frank et al., 1981*b*).

Arrangement of subfilaments along the length of the filament

Three serial transverse sections 110 nm thick were used for this study. These sections were of muscle fixed under 200 mM rigor conditions. An area containing 60 filaments was analyzed. The 60 images in each section were processed to obtain the threefold center for each.

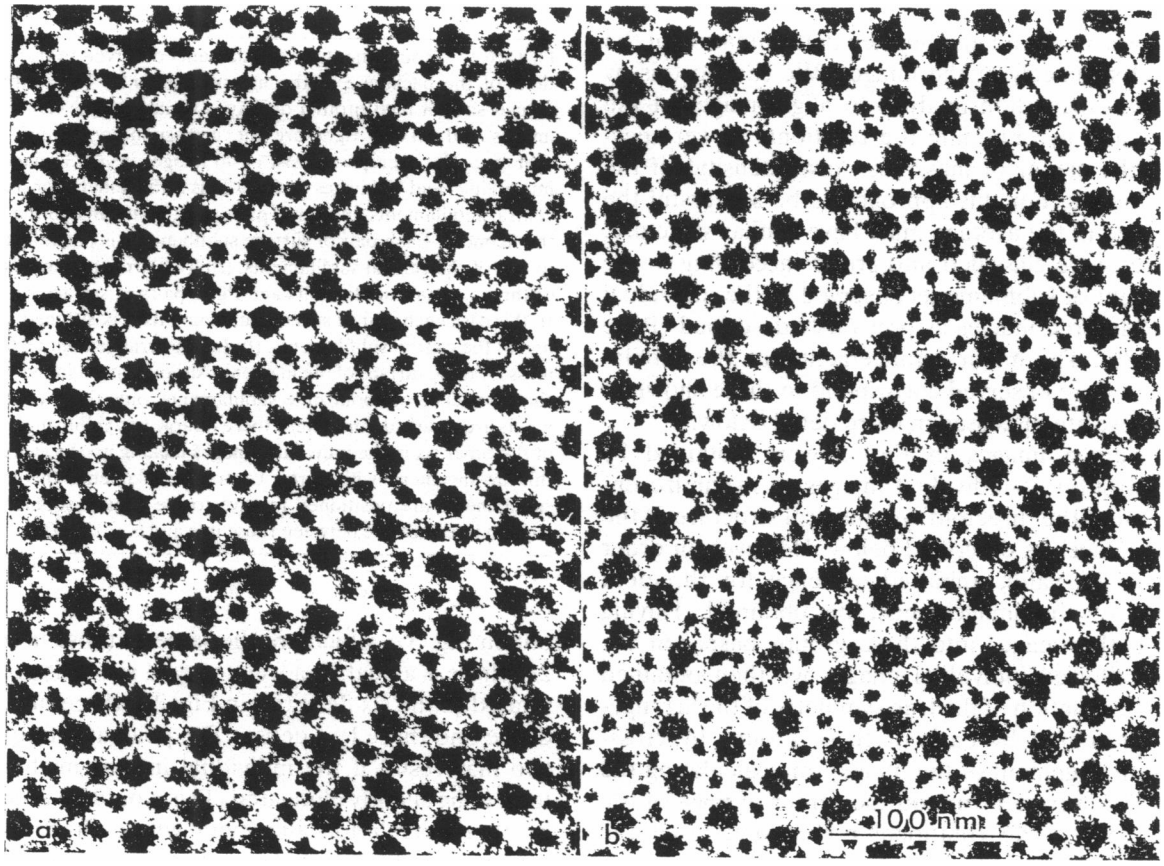

FIGURE 1 Transverse sections of skinned muscle fibers. The skinned fibers were fixed at an ionic strength of 200 mM under (*a*) rigor and (*b*) relaxed conditions (see text). The lattice arrangement is much more regular in the rigor muscle than in the relaxed muscle. The thin actin containing filaments appear thicker in the rigor muscle than in the relaxed. ×250,000.

Averaging of the three serial images of the same filament was done on the threefold center without rotation of the images.

RESULTS

Representative examples of the transverse sections used in this work are shown in Fig. 1. The tissue was fixed at an ionic strength of 200 mM. At the time of fixation, for one case the muscle was in rigor (Fig. 1 *a*) and for the other relaxed (Fig. 1 *b*). The lattice arrangement is much more regular in the rigor muscle than in the relaxed muscle. The disorder in the relaxed muscle appears to be greater for the position of the actin filaments than for that of the myosin filaments in the lattice. The actin filaments in the rigor muscle appear to be thicker than those in the relaxed muscle, consistent with the binding of myosin cross-bridges to the actin filaments under rigor conditions but not under relaxing conditions.

Symmetry of the images and averaging

Our aim was to obtain an unbiased determination of the rotational symmetry of the images. We can do this by using cross-correlation analysis to align images of the filaments and by obtaining the rotational power spectrum on the center of mass (i.e., pixel density) of the average images. For this approach to be successful the images used in the average must have similar structure. All images were classified into groups according to the arrangement of subfilaments observed in the individual threefold filtered images as previously described (Pepe et al., 1986). The major arrangements for the subfilaments that were observed correspond to those shown in Fig. 2. These are discussed in more detail below.

The average images in Fig. 2 were obtained by superimposition of individual images to maximize enhancement of the threefold symmetrical structure of the group of images as described below. However, in order for this to be valid, unbiased evidence for threefold symmetry of the images must be obtained. Having separated the images into these groups based on the threefold filtered individual images we then obtained unbiased evaluation of the true symmetry of the arrangement represented by each of these groups by cross-correlation alignment of the images and calculating the rotational power spectrum on the center of mass of the average image. The rotational power spectra of the cross-correlation–aligned average images are shown in Fig. 3, *a*, *b*, and *c*. For the two groups of images used to obtain Fig. 3, *a* and *b*, which are the same as those used in Fig. 2, *a* and *b*, the power spectra have strong threefold symmetry. For the group of images used to obtain Fig. 3 *c*, which are the same as those used in Fig. 2 *c*, there is a peak at a frequency of six. This probably is related to the six densities in Fig. 2 *c*, three of which are dense and three less dense. The peak at a frequency of two may result if the individual images in the average tend to be slightly elongated. This would be accentuated by cross-correlation alignment where shape is heavily weighted in the alignment procedure. Using different reference images from each group for the cross correlations gave similar results.

To test the symmetry further, we decided to weight the cross-correlation alignment of the images by using a

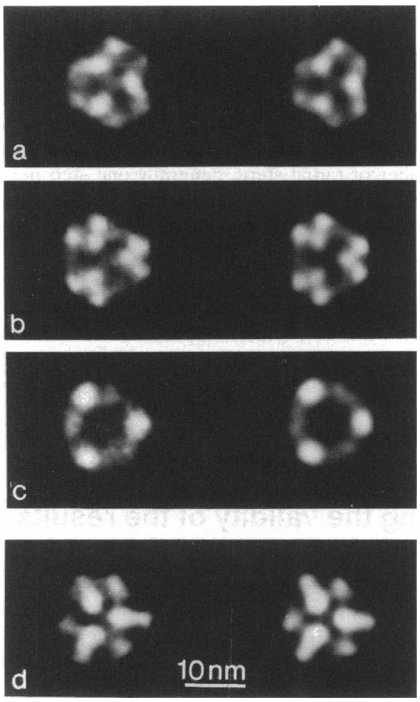

FIGURE 2 Arrangements of subfilaments observed in transverse sections of the backbone of the myosin filaments. These are negative images so that high protein density is white. On the left are average images and on the right are the corresponding threefold filtered averages. The averages consist of 70 images in *a*, 73 images in *b*, 76 images in *c*, and 70 images in *d*. (*a*) This arrangement consists of three central subfilaments and three pairs of subfilaments on the surface of the filament. Each pair of surface subfilaments is positioned adjacent to two of the central subfilaments. (*b*) This arrangement also consists of three central subfilaments and three pairs of surface subfilaments. In this case each pair of surface subfilaments is positioned adjacent to one of the central subfilaments. (*c*) In this arrangement all the protein mass is on the surface of the filament. Although most individual images show evidence of about nine subfilaments, only three of the subfilaments are clearly defined since there is large variability in the positions of the other six in the individual images making up the average. (*d*) In this arrangement with three central subfilaments the six surface subfilaments are positioned relative to the central subfilaments in a pattern intermediate between those in *a* and *b*. ×750,000.

rotationally filtered image as the reference for the alignment. We used the same group of images as was used for obtaining Fig. 3 *a*, only now the reference image was rotationally filtered for three-, four-, five-, or sixfold symmetry. The power spectra for the averages obtained after corss-correlation using the rotationally filtered reference images are shown in Fig. 3, *d*, *e*, *f*, and *g*. When the threefold filtered image was used as a reference, the power spectrum (Fig. 3 *d*) is essentially the same at that obtained using the unfiltered image as a reference (Fig. 3 *a*). Using the four- or fivefold filtered reference image (Fig. 3, *e* and *f*) there is no peak in the power spectrum corresponding to the symmetry imposed on the reference image, suggesting that these symmetries are not present in the individual images aligned by cross correlation. Alignment of the images against a fourfold filtered image (Fig. 3 *e*) gave a peak at a frequency of 2 rather than 4. This could result if the individual images in the average are slightly elongated because shape contributes significantly to the cross-correlation alignment. Another possibility is the fact that the individual images used for obtaining Fig. 3, *a*, *d*, *e*, *f*, and *g*, which are those that were averaged in Fig. 2 *a*, are already similarly oriented rotationally on their threefold centers. Cross correlating these similarly oriented threefold images with the fourfold reference image could result in alignment of the images in either of two directions. Cross correlation of randomly oriented threefold images with a fourfold reference would be expected to give an average with the fourfold symmetry of the reference. On trying to impose fivefold symmetry using these same images, a peak at a frequency of 3 was obtained (Fig. 3 *f*). In this case it appears that the similarly oriented images were all realigned in the same way leading to an average with the threefold symmetry of the individual images. Again if the images had been randomly oriented the average of the cross correlation aligned images would be expected to have fivefold symmetry. Cross-correlation alignment with respect to a sixfold filtered reference image (Fig. 3 *g*) gave peaks at frequencies of 6 and 2. The frequency of six results from alignment of the individual images with either one or the other densities 60° apart in the sixfold reference image. The frequency of 2 probably reflects the presence of individual images with slightly elongated profiles as suggested above.

In addition to the cross-correlation analysis we also evaluated symmetry of the individual images by studying the power spectrum obtained using centers where *n*-fold

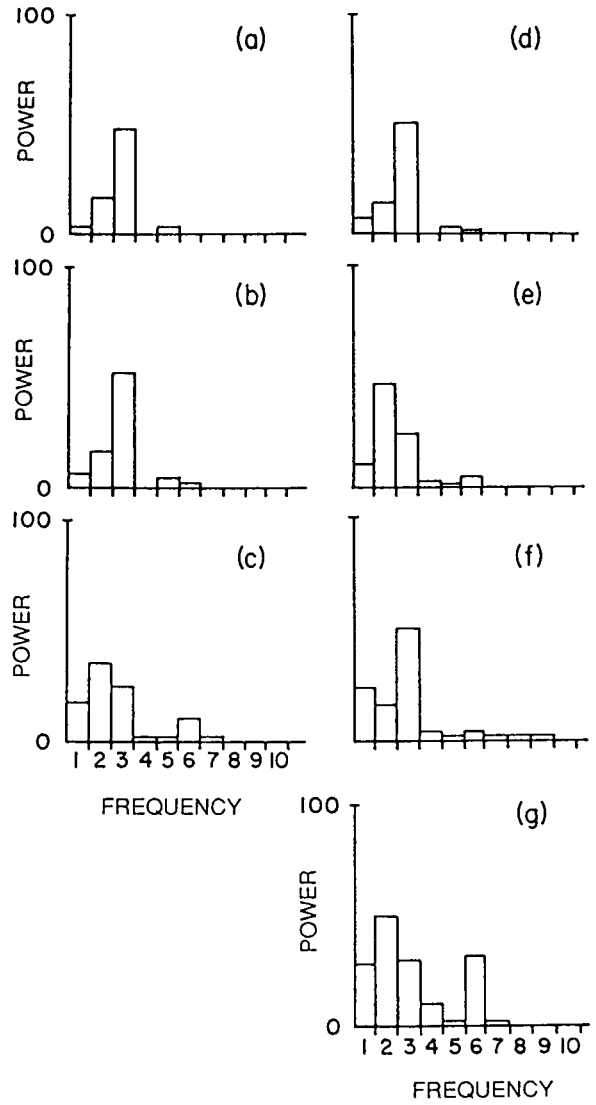

FIGURE 3 Cross-correlation alignment and averaging of images. Images were aligned by cross correlation for averaging and the rotational power spectrum on the center of mass (pixel density) was obtained. (*a*) Rotational power spectrum from the cross-correlation alignment and averaging of the images also used in Fig. 2 *a* (where they were aligned on their threefold centers). Note the peak of power at a frequency of 3. (*b*) Rotational power spectrum from the cross correlation alignment and averaging of the images also used in Fig. 2 *b*. Note the peak at a frequency of 3. (*c*) Rotational power spectrum from the cross correlation alignment and averaging of the images also used in Fig. 2 *c*. Note the peak at a frequency of 6. There is also power at frequencies of 1, 2, and 3. (*d*) Rotational power spectrum from the cross-correlation alignment and averaging of the images also used in Fig. 2 *a*; obtained as for *a* except that the reference image was filtered for threefold symmetry using frequencies of 3, 6, 9, 12, and 15. This had no significant effect on the power spectrum. (*e*) Same as *d* except that the reference image was filtered for fourfold symmetry using frequencies of 4, 8, 12, and 16. There is no peak at a frequency of 4 in this attempt to bias the results in favor of fourfold symmetry. (*f*) Same as *d* except that the reference image was filtered for fivefold symmetry using frequencies of 5, 10, 15, and 20. There is no peak at a frequency of 5 in this attempt to bias the results in favor of fivefold symmetry. (*g*) Same as *d* except that the reference image was filtered for sixfold symmetry using frequencies of 6, 12, and 18. There is a peak at a frequency of 6 which is a harmonic of threefold symmetry.

power was the maximum percentage of total (nonzero) power. This was done on a group of 60 images, taken from an area of a section, for values of n from 3 to 9 using muscle fixed under 200 mM rigor conditions. It was found that the number of filaments for which there was a peak in the power spectrum at frequency n was largest when n was 3. In this case ~80% of the images met this criterion with the other 20% having some structural disorder. This is consistent with filament images that have threefold symmetry. In Fig. 4, *a*, *b*, and *c*, power is plotted as a function of frequency for three individual images representative of those observed. In each case there is relatively strong power at a frequency of 3. The percent of total nonzero power that is threefold in the individual images ranged from 23% to 55%

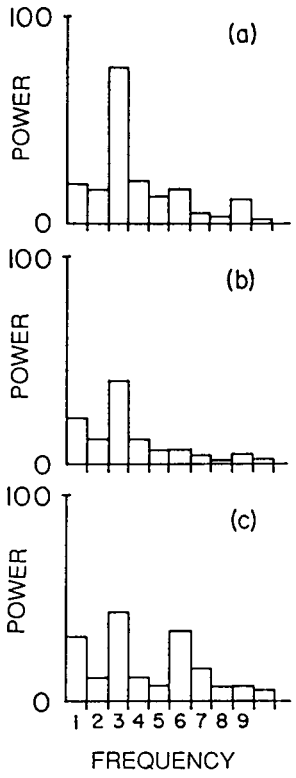

FIGURE 4 Rotational power spectrum of representative individual images of transverse sections of myosin filaments. These were taken from a group of 60 images, 80% of which had power spectra that showed evidence for threefold symmetry. The images were filtered for threefold symmetry using the center where threefold power was the highest percentage of total nonzero power. (*a*) There is a strong peak at a frequency of 3 in this image. The power at the frequency of 3 and its harmonics, i.e., total threefold power, represents 70% of the total nonzero power. (*b*) The peak at the frequency of three in this image is not as large as that in *a*. The total threefold power represents 46% of the total nonzero power. (*c*) For this image there is a peak at a frequency of 3 and another at a frequency of 6 which is a harmonic of 3. The total threefold power represents 48% of the total nonzero power.

As a result of these findings and other studies addressed in the discussion we feel reasonably confident that the images we are dealing with have threefold symmetry. Therefore alignment and filtering procedures which enhance the threefold structural symmetry in the images are valid. The individual images were therefore superimposed on their threefold centers and rotationally aligned for maximum superimposition of their subfilaments as described previously (Pepe et al., 1986) and the resulting average images are those in Fig. 2. The power spectra for the three average images are shown in Fig. 5, *a*, *b*, and *c*. Comparing the power spectra of average images aligned by cross correlation in Fig. 3, *a* and *b*, with the corresponding Fig. 5, *a* and *b*, shows that they are very similar with the major difference being enhancement of the threefold power in Fig. 5, *a* and *b*, and the harmonic at a frequency of 6 now showing up. The power spectrum obtained by cross-correlation alignment in Fig. 3 *c* and that obtained by aligning on the threefold centers in Fig. 5 *c* are not as closely similar. In both alignments there is a peak at a frequency of 6 which is enhanced by the threefold alignment. In Fig. 5 *c* where alignment was on the threefold center there is also a strong peak at a frequency of 3, which is not present on cross-correlation alignment (Fig. 3 *c*). As suggested earlier the peak at a frequency of 2 obtained by cross-correlation alignment (Fig. 3 *c*) could be due to the strong influence of the transverse profile or shape of the image on the alignment. A slight elongation of the subfilament arrangement could lead to significantly increasing the contribution of the threefold symmetry on cross-correlation alignment (Fig. 3 *c*). Alignment of the images on the threefold center of the subfilament arrangement with rotational alignment to maximize superimposition of the subfilaments will minimize the contribution of filament shape to the alignment and would lead to an increase in the contribution of the threefold subfilament arrangement to the frequency distribution of power as seen in Fig. 5 *c*. The validity or reproducibility of these averages on the threefold center (Fig. 2) was assessed by comparing the averages obtained by two independent sets of images (Frank et al., 1981*b*) as shown in Fig. 6. Two independent sets of the images in Fig. 2 *b* were shown to be structurally similar and the variance and standard deviation of the averages were shown to be small.

Subfilament organization in transverse sections

The three arrangements of subfilaments in Fig. 2, *a*, *b*, and *c*, were present in all three regions along the length of the filament, i.e., and P, C, and D regions for all of the conditions used in this study, i.e., 200 mM relaxed and

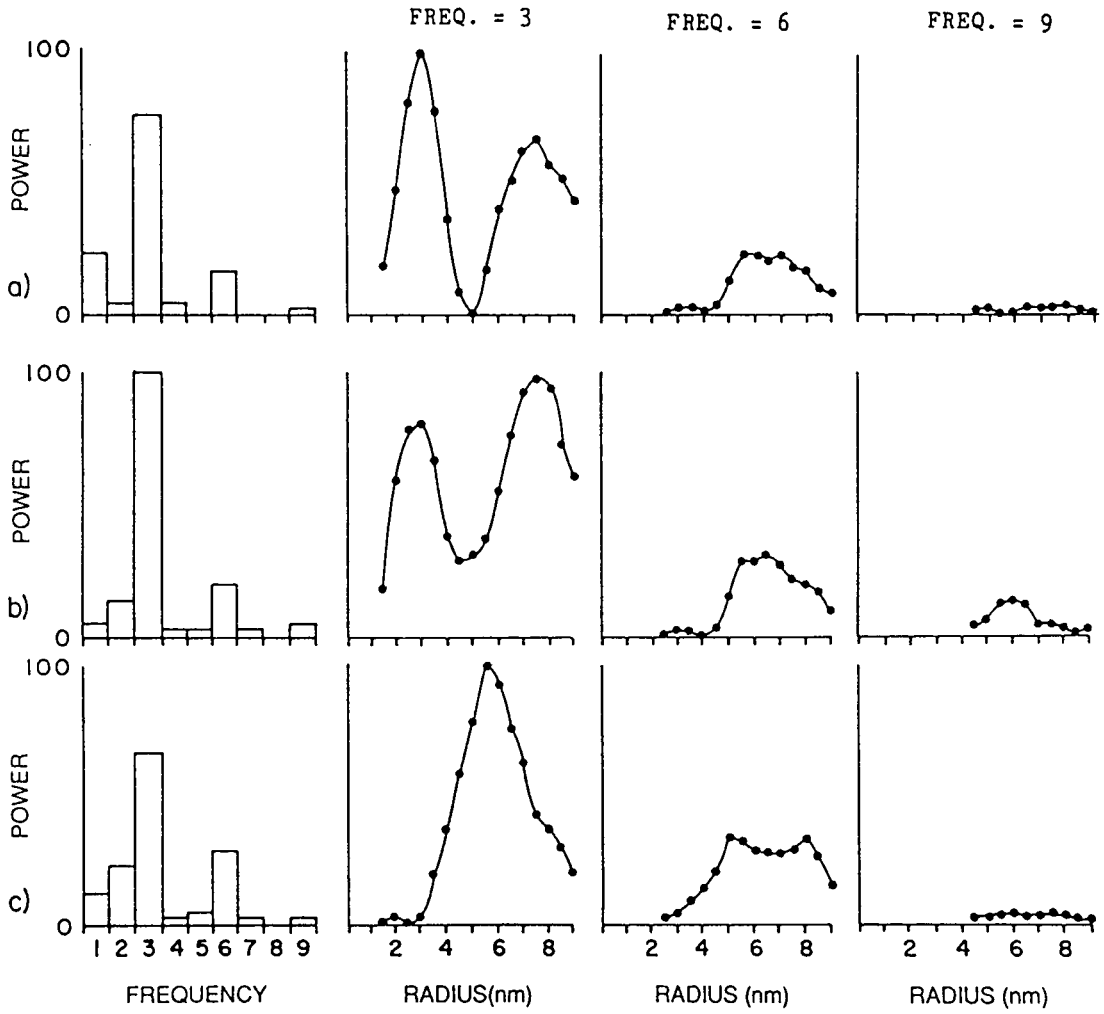

FIGURE 5 Rotational power spectrum of average images superimposed on their threefold centers and rotationally oriented for maximum superimposition of subfilaments. The graphs in *a* correspond to the average image in Fig. 2 *a*, those in *b* to the average image in Fig. 2 *b*, and those in *c* to the average image in Fig. 2 *c*. In the first column is the power as a function of frequency. The second, third, and fourth columns are power as a function of radius for frequencies of 3, 6, and 9, respectively. In all three averages there are peaks of power at frequencies of 3 and 6 (first column). In the second column the averages for *a* and *b* show two peaks of power as a function of radius for a frequency of 3. The peak at 3 nm in *a* and that at 2.75 nm in *b* correspond to the position of the three central subfilaments in Fig. 2, *a* and *b*. The peaks at 7.5 nm in *a* and *b* correspond to the three pairs of surface subfilaments in Fig. 2, *a* and *b*. In *c* there is one peak at a radius of 6 nm corresponding to the position of the three dense subfilaments and the density between them in Fig. 2 *c* which are all at the surface. In the third column for a frequency of 6 there is a broad peak of power from ~5 to 8 nm for all three averages. Only in *b* is there any detectable power at a frequency of 9 occurring at a radius of ~6 nm.

rigor, and 20 mM AMPPNP. Two of the arrangements are characterized by three central subfilaments and three pairs of subfilaments on the surface for a total of nine subfilaments (Fig. 2, *a* and *b*). In the third arrangement all nine subfilaments are on the surface (Fig. 2 *c*). In the average image in Fig. 2 c only three densities are strong. These correspond to three of the nine subfilaments observed on the surface of the filament in the threefold filtered versions of the individual images which formed the average (using the three cycles of alignment of unfiltered images as described in Materials and Methods). These three subfilaments did not vary in position from image to image as much as the other six subfilaments and therefore could be most easily superimposed. The lighter density between the three strong densities in Fig. 2 *c*, results from the other six more variably placed subfilaments on the surface of individual images. This is responsible for the observed strong threefold symmetry in Fig. 5 *c* rather than a ninefold symmetry that would be expected if all nine of the subfilaments observed in the individual images could be similarly superimposed in the average. At the higher

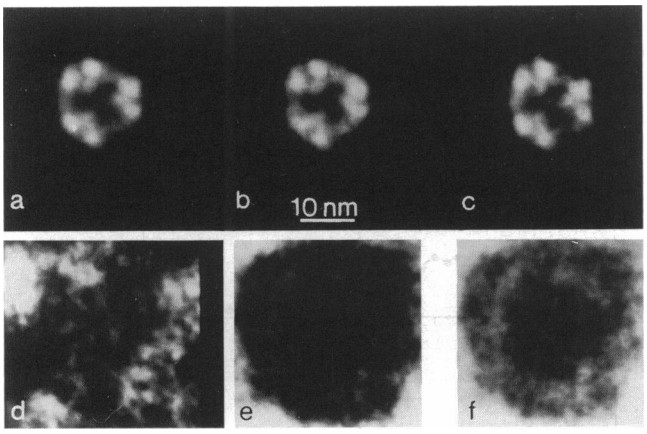

FIGURE 6 Assessment of validity of the average images in Fig. 2. To do this we split the 73 images used in the average in Fig. 2 *b* into two independent sets of images (Frank et al., 1981*b*). (*a*) Same as Fig. 2 *b*. Because this is a negative image, the highest protein density is white. (*b*) Average of 37 of the images used in *a*. (*c*) Average of the other 36 of the images used in *a*. The averages in *b* and *c* are structurally similar. (*d*) Difference image obtained by subtracting *b* from *c*. In the center of the difference image corresponding to the position of the filament, the small differences are not significant (less than three times the standard error of the average image in *a*). The large differences observed peripherally are artifacts of the superimposition of the individual images in the averages. (*e*) Variance map of the average in *a*. The variance in the area of the filament is very small. The increase peripherally is due to artifacts of the superimposition of images in the average. (*f*) Standard deviation of the average in *a*. This is low in the region of the filament and especially low in the areas where the subfilaments are located.

ionic strength (200 mM) used for the relaxed and rigor conditions, a variation of the arrangements in Fig. 2, *a* and *b*, was also observed (Fig. 2 *d*). This consisted of a shift of the pairs of subfilaments on the surface relative to the three central subfilaments such that one subfilament of each pair is juxtaposed with a central subfilament. This variation appeared to be intermediate to the arrangements in Fig. 2, *a* and *b*. In the P region, the shift was always clockwise, whereas in the C and D regions, the shift could be clockwise or counterclockwise in the same section. All images were viewed looking from the M-band toward the Z-band. These variations were only rarely seen at 20 mM ionic strength in the presence of Mg AMPPNP. At 200 mM ionic strength, the representation of the four different arrangements for both relaxed and rigor conditions was about the same in the three regions along the filament. An average of 18% of the images had the arrangement in Fig. 2 *a*, ~13% the arrangement in Fig. 2 *b*, with 36% having the intermediate arrangement (Fig. 2 *d*), and 33% the arrangement in Fig. 2 *c*. At an ionic strength of 20 mM in the presence of Mg AMPPNP the representation of the arrangements in Fig. 2 changed with the region of the filament. The arrangement in Fig. 2 *b* was more prevalent in the P region (64%) than the D region (22%), and the arrangement in Fig. 2 *a* was more prevalent in the D region (33%) than in the P region (12%). They were about equally represented in the C region (34–42%). The arrangement in Fig. 2 *c* was also more prevalent in the D region (45%) than in the P region (23%).

In Fig. 5, in addition to power as a function of frequency, the power as a function of radius is plotted from the power spectra for the average images in Fig. 2. In Fig. 5, *a* and *b*, the power as a function of radius for a frequency of 3 shows two peaks. In Fig. 5 *a* one peak is at a radius of 3 nm corresponding to that in Fig. 5 *b* at a similar radius of ~2.75 nm. The value of 2.75 nm was obtained by averaging the radii corresponding to the two points at the top of the peak, i.e., 2.5 and 3.0 nm. These peaks correspond to the radial position of the three central subfilaments. The other peak in both cases is at a radius of ~7.5 nm, corresponding to the surface of the filament. In Fig. 5 *c*, where all the protein density of the subfilaments is on the surface, the peak of radial density at a frequency of 3 is at a radius of ~6 nm, with a broader shoulder on the peak with increasing radii to the surface of the filament. For a frequency of 6, the power as a function of radius is in a rather broad peak over radii from ~5 to 8 nm for all three arrangements, reflecting the contribution of the surface subfilaments to the symmetry. Only in Fig. 5 *b* was there any detectable power at a frequency of 9 and this occurred at a radius of ~6 nm.

Although the arrangements of subfilaments in the average images in Fig. 2 were different, the diameters of the filaments were the same. The diameter was determined by taking the first derivative of the radial density distribution of the images. These curves are shown in Fig. 7 where the radial density distributions are plotted in *a*, and the first derivative in *b*. The edge of the filament is represented by the peak of the first derivative of the radial density distribution. For the average images in Fig. 2, *a* and *b*, this occurs at a radius of 8 nm (diameter 16 nm) and for that in Fig. 2 c at a radius of 8.5 nm (diameter 17 nm). Therefore the diameter of the filament is essentially the same regardless of the arrangement of subfilaments in the backbone.

To determine whether the three arrangements of subfilaments in Fig. 2 are significantly different, the average images were subtracted from each other and the statistical significance of the difference image were determined from the variations in pixel density among the images making up each group. In Fig. 8 *a* the average from Fig. 2 *a* is shown in the middle, that from Fig. 2 *b* is shown on the left, and the difference image obtained by subtracting the middle image from that on the left is

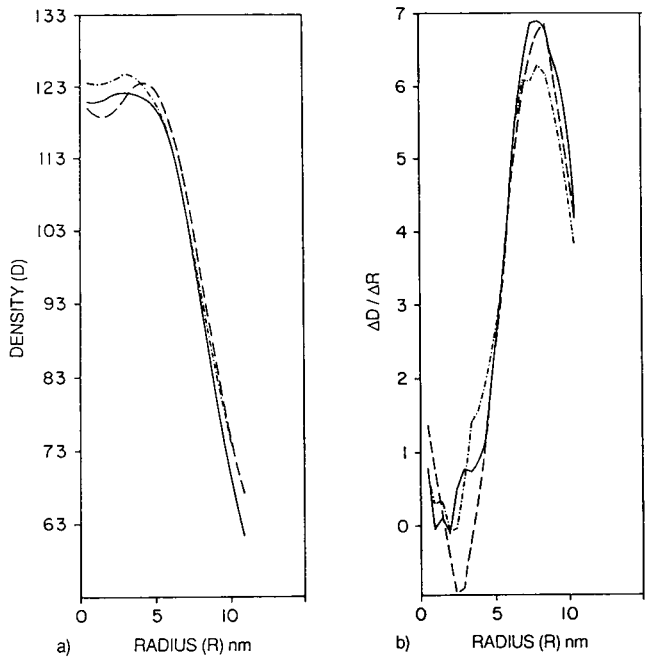

FIGURE 7 Determination of the edge of the filament. (*a*) The radial density distributions for the three average images in Fig. 2, *a*, *b*, and *c*, are shown. The solid line is for that in Fig. 2 *b*, the dashed line for that in Fig. 2 *c*, and the dot and dashed line for that in Fig. 2 *a*. (*b*) The corresponding curves for the first derivative of the radial density distributions in *a* are shown. The peaks of these curves correspond to the edge of the filaments. The peaks vary from 8 to 8.5 nm, meaning that the diameter of the three average images in Fig. 2, *a*, *b*, and *c*, are essentially the same and that the diameter therefore does not change with change in the arrangement of the subfilaments.

shown on the right. The criterion used for assessing the significance of the difference image is described in Materials and Methods. On the left in Fig. 8 *b* is an image representing the significant density difference, i.e., the density of the difference image from which was subtracted three times the standard error of each pixel of the average image above it in Fig. 8 *a* and similarly in the middle in Fig. 8 *b* is the same difference image after subtracting three times the standard error at each pixel of the image above it in Fig. 8 *a*. On the right in Fig. 8 *b* is the standard error map of the difference image above it in Fig. 8 *a*. Note that the significant parts of the difference image (Fig. 8 *b*, middle and left) are in an area of very low standard error in the difference image. This same process was carried out in Fig. 8, *c* and *d*, and in Fig. 8, *e* and *f*. From Fig. 8, *a* and *b*, it is clear that there is a significant difference in the position of the surface subfilaments in the two arrangements which have three central subfilaments. From Fig. 8, *c–e*, it is clear that there is a significant difference between the arrangements with three central subfilaments and the arrangement in which all subfilaments are arranged on the surface of the filament.

As a control on the studies of how significantly different the observed arrangements in Fig. 8 were average images of groups of filaments with the same arrangement of subfilaments obtained from different regions along the length of the filament were subtracted in the same way as was done for the different images in Fig. 8. Regardless of the arrangement of subfilaments, in general, no significant difference was observed on subtracting different averages of groups with the same arrangement of subfilaments from each other. Therefore there is no significant variation of the arrangement of subfilaments within the groups of average images obtained by this procedure. This further strengthens the validity of our sorting of the images into these groups with different arrangements.

Lattice arrangement

The rotational alignment on the threefold center of individual images for maximum superimposition of subfilaments (Fig. 2) was done by clockwise rotation only (Pepe et al., 1986). Therefore the frequency distribution of angular rotation should give information about the relative angular positioning of neighboring filaments in the lattice. The analysis was done using 10° bins combining the results of three different experiments, all fixed under 200 mM rigor conditions, with the same lattice orientation for a total of 469 images (32% required a rotation from 0° to 9° for superimposition on the threefold center and 15% required 90°–99° rotation). The other bins are all in the range of 4–8% except for 110°–119° where there were 1%. This suggests that there is a preferential orientation around 0° and 90°. The angles of rotation were mapped on the lattice in an attempt to define this preferential orientation in terms of a superlattice arrangement. Images were always viewed looking from the M-band toward the Z-band. The relative position of the filaments with similar angular orientation in the lattice were found to be random and no ordered superlattice could be defined. Similar results were found for the different conditions studied.

Resolution

The phase residual test for resolution (Frank et al., 1981 *b*; Van heel, 1987) was applied to the images used here. A group of 60 images with the arrangement of subfilaments shown in Fig. 2 *a* was split into two groups of 30 images each. The phase residual was calculated between one image of each group and then for the cumulative average obtained by successively adding an

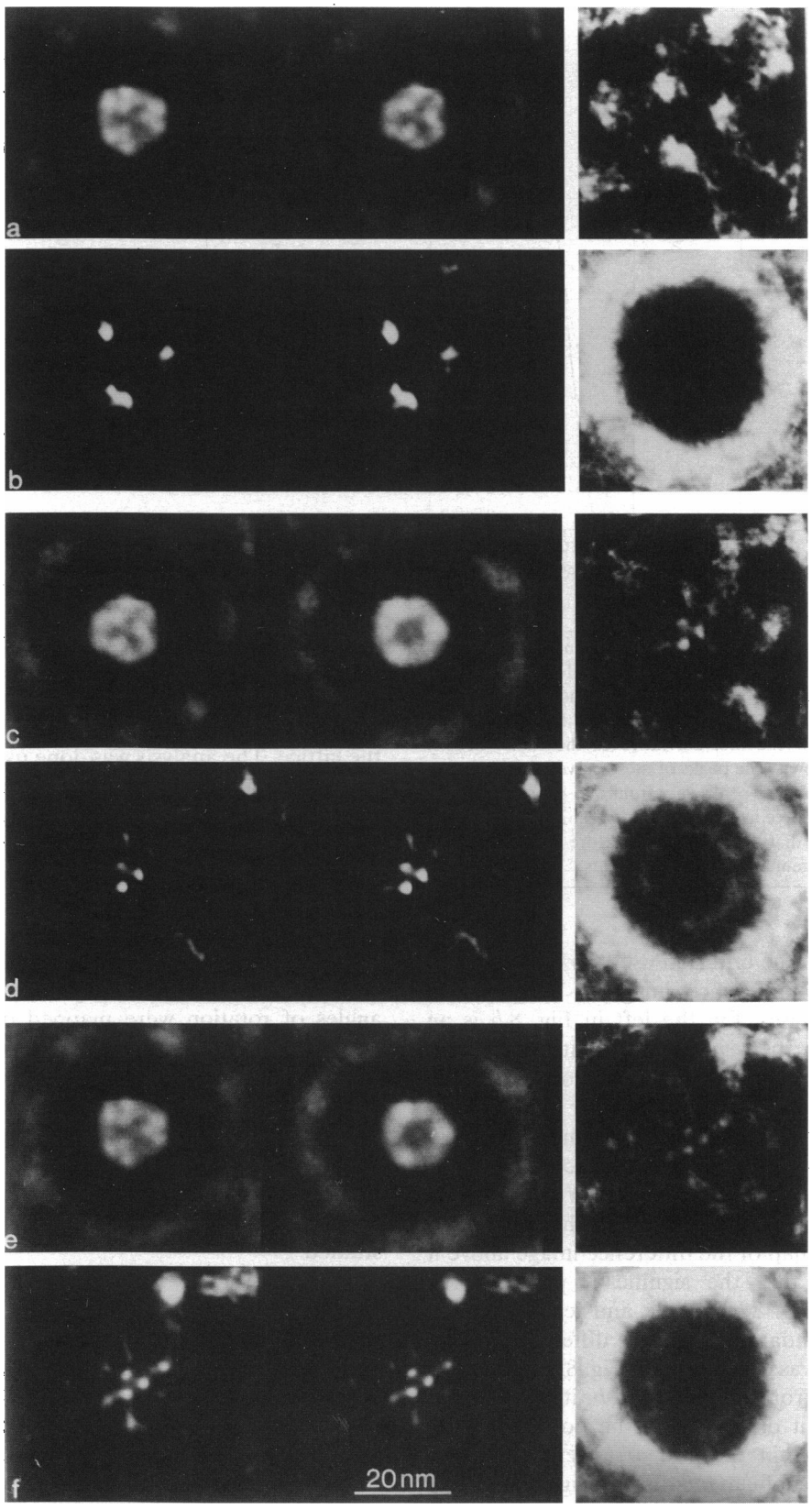
a
b
c
d
e
f
20 nm

image to each group. The averages were determined on the threefold center rotationally aligned for maximum overlap of the subfilaments in individual images (as in Fig. 2 *a*). The phase residual was calculated for each cumulative average for 10 Fourier rings corresponding to resolutions from 2.5 to 8 nm. The maximum acceptable phase residual of 45° (Frank et al., 1981*b*) was reached at a resolution of 3.5 nm (Fig. 9) with the averaging of 18 images in each group. At a resolution of 3.2 nm the averaging of ~26 images in each group brought the phase residual very close to 45°, suggesting a resolution between 3.2 and 3.5 nm. Since this is a conservative method for determining resolution (Van Heel, 1987), the actual resolution in the average images is probably better.

Arrangement of subfilaments along the length of the filament

Although the different arrangements of subfilaments shown in Fig. 2, *a*, *b*, and *c* (fixed under 200 mM rigor) are present in all regions along the length of the filament it is not clear how the transition from one to the other occurs. To determine this, three serial sections (110 nm thick) were examined following the same filament in each serial section. An area of the lattice containing 60 filaments was studied in this way. The definition of subunits was not equally good in all three of the serial sections required to follow the same filaments. In each section ~80% of the filaments had threefold symmetry. in 27 of the 60 filaments all three serial sections had threefold symmetry. It was found that the images in the three serial sections of one filament did not generally have the same arrangement of subfilaments and no meaningful change in the arrangement from one section to the next could be found.

The 27 filaments in which all three serial sections had threefold symmetry were studied further. The first of these sections was in the P region at the boundary between the P and C regions, and the next two sections were in the C region. The images in the three serial sections of a filament were superimposed (total thickness of 330 nm) on the threefold center and averaged without rotation relative to each other. Of the 27 average images, six did not have threefold symmetry even though the three individual images averaged for each filament did have threefold symmetry. Therefore, in these six filaments the change in subfilament positions from section to section was great enough that the threefold symmetry was lost. In 21 of the 27 images, or 78%, the subfilament arrangement from section to section was such that the average image had threefold symmetry. In these images with threefold symmetry, there were sixteen with three central subfilaments as in the arrangements in Fig. 2, *a* and *b*, and five with the arrangement in Fig. 2 *c*. With this small number of images we did not try to distinguish between the arrangements in Fig. 2, *a* and *b*.

DISCUSSION

There is considerable evidence for threefold structural symmetry in the vertebrate skeletal myosin filament. In this study we provide further evidence for this symmetry, and we examine in more detail the arrangement of subfilaments in the filament backbone. An important consideration in these studies is tissue preservation, including preservation of the detailed backbone structure in the myosin filament. In the past we have evaluated resolution and structure preservation in electron micrographs of the myosin filament backbone using the optical diffraction patterns of images of transverse sections of individual myosin filaments (Pepe and Dow-

FIGURE 8 Verification of the significance of the differences observed in the average images in Fig. 2. These are negative images. Therefore white is high density. (*a*) The average from Fig. 2 *a* is in the middle and that from Fig. 2 *b* is on the left. On the right is the difference image obtained by subtracting the middle image from that on the left. (*b*) On the left is the result of taking the difference image in *a* (right) and subtracting from it three times the standard error of each pixel in *a* (left) which is above it. Similarly for the middle image. In this case three times the standard error of each pixel in *a* (middle) was subtracted from the difference image in *a* (right). These images represent the significant density for the difference image in *a* (right). On the right is a map of the standard error of the difference image above it in *a* (right). Note that the area of low standard error in the difference image corresponds to the area in which there is significant difference in the images (*a*, left and middle). The significant difference in the images corresponds to the surface of the filament and reflects the difference in position of the three pairs of surface subfilaments in the two images. (*c*) The average from Fig. 2 *a* is on the left and that from Fig. 2 *c* is in the middle. On the right is the difference image obtained by subtracting the middle image from that on the left. (*d*) These images were obtained in the same way as those in *b*. The significant difference in the images (left and middle) corresponds to the area of low standard error for the difference image (right). The significant difference corresponds mainly to the middle of the filament reflecting the presence of three of the subfilaments in the middle of the filament in one arrangement and the presence of all subfilaments on the surface of the filament in the other. (*e*) The average from Fig. 2 *b* is on the left and that from Fig. 2 *c* is in the middle. The difference obtained by subtracting the middle image from that on the left is shown on the right. (*f*) These images were obtained in the same way as those in *b* and *d*. The results are the same as those obtained in *d* showing that the major difference between the two average images is the presence of central subfilaments in one and not the other. ×700,000.

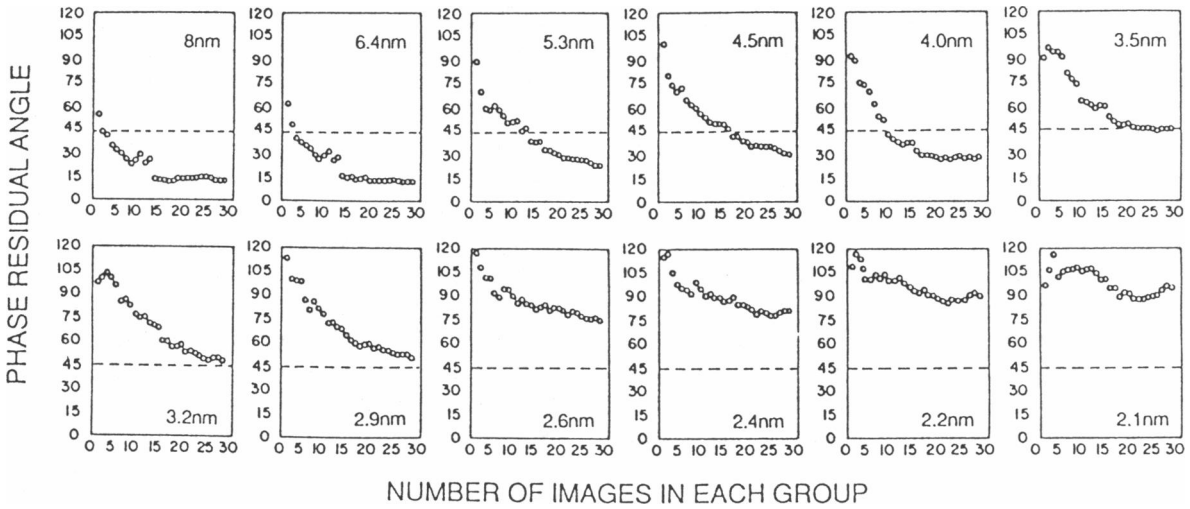

FIGURE 9 Phase residual test for resolution. This test was carried out for the images in the average shown in Fig. 2 *a*. Of the 70 images in this group, the first 60 images were separated into two groups of 30 and the phase residual was calculated between one image from each group and then for the cumulative average obtained by successively adding an image to each group. The successive images were aligned for averaging as was done for the images used in Fig. 2 *a*. By using a maximum acceptable phase residual of 45° (Frank et al., 1981*b*), a resolution of 3.5 nm was obtained. Note that for 3.5 nm resolution, the averaging of 18 images in each group gives a phase residual of 45°, and at a resolution of 3.2 nm, the averaging of 26 images brings the phase residual close to 45°. Therefore the resolution is probably between 3.2 and 3.5 nm.

ben, 1977; Pepe et al., 1981; Ashton and Pepe, 1981; Stewart et al., 1981). Because there may be contributions to the optical diffraction patterns from the shape of the filament image, we also analyzed the images using the autocorrelation map (Pepe et al., 1981; Stewart et al., 1981; Pepe et al., 1986), which represents the distribution of spatial vectors in the image and is more dependent on regular internal structure than on the shape of the image. In those studies, substructure spacings of 3–4 nm were measured. We have now applied more stringent tests of the validity of these findings and we have shown by applying the phase residual test for resolution (Frank et al., 1981*b*) that average images have a resolution of at least 3.2–3.5 nm.

Throughout this study we have used sections 110 nm thick, whereas in previous work, sections 140–300 nm thick (Pepe and Dowben, 1977; Pepe et al., 1981; Stewart et al., 1981) were used. The danger of using thick sections is that the background phase granularity, which is related to microscope defocus, could be confused with image structure. Using sections 140 nm thick and taking a thorough focal series of micrographs of the same filament, we showed that there was essentially no change in the optical diffraction pattern of the images over a focal range of 198 nm (Pepe et al., 1981). This makes it highly unlikely that the substructure in the images arises from the focal level of the microscope. With the thinner sections, 110 nm thick, used in this study, this possible source of artifact is still further diminished.

At the higher ionic strength of 200 mM both rigor and relaxed conditions were studied. An important finding was that the backbone structure of the filaments was not different under these different conditions. The different arrangement of subfilaments observed in the backbone was the same and the relative proportion of the different arrangements observed in different regions along the length of the filament did not change under relaxed and rigor conditions. Therefore attachment of the myosin cross-bridges to the neighboring actin filaments in rigor does not produce detectable perturbations of the backbone structure observed under relaxed conditions where the myosin cross bridges are not attached to the actin filaments. The structures observed at the lower (20 mM) ionic strength that was studied were also observed at the higher (200 mM) ionic strength.

Symmetry

All vertebrate myosin filaments studied so far show evidence for threefold symmetry either in their subfilament organization, the triangular transverse profiles in the M-band region, in the helical arrangement of myosin cross bridges on the surface of the filament or in the splaying of separated filaments into three parallel units under appropriate conditions (Maw and Rowe, 1980; Pepe, 1982). The subfilament organization of fish muscle

myosin filaments (Stewart et al., 1981; Pepe et al., 1986) is the same as that in the chicken muscle filaments (Pepe and Drucker, 1972) studied in this work. In contrast, the relative orientations of the triangular transverse profiles are all the same in fish muscle (Pepe, 1971, 1982; Pepe and Dowben, 1977; Luther et al., 1981) but are different in chicken muscle (Pepe and Drucker, 1972) where they are related by about a 60° or 180° rotation similar to what has been observed in frog muscle (Luther and Squire, 1980; Luther et al., 1981). Luther et al. (1981) have directly compared the superlattice arrangement previously described in the frog (Luther and Squire, 1980) with the absence of any superlattice in the fish. Evidence for a threefold helical symmetry of the myosin cross bridges on the surface of the myosin filaments has been obtained for fish (Varrano-Narston et al., 1984), frog (Stewart and Kensler, 1986; Kensler and Stewart, 1986; Cantino and Squire, 1986) and rabbit (Ip and Heuser, 1983; Knight et al., 1986) muscles. Therefore, although the subfilament arrangement and the myosin cross-bridge helical symmetry is the same in the different muscles studied so far, the relative orientation of the transverse triangular profiles in the fish in different from that of the other muscles (chicken and frog) studied so far. Unpublished observations of rabbit muscles (C. Owen, J. Frank, J. Weisel, and F. Pepe) show them to be similar to the chicken and frog in the relative orientation of the triangular transverse profiles.

Evidence suggesting that the symmetry of the subunit organization of the myosin filament backbone is threefold includes optical diffraction and autocorrelation analysis on images of transverse sections of individual filaments (Pepe et al., 1981) as well as back projection and rotational averaging methods (Stewart et al., 1981; Pepe et al., 1981). Although the symmetry of the myosin cross bridge arrangement need not be the same as that of the backbone, they do need to be related. The splaying of the filament into three parallel units and the triangular shape of the transverse profile of the filament, while strongly indicating a threefold structure, say nothing further about the substructure.

The question of the symmetry of the images of the subfilament arrangement in the backbone has been reexamined using cross-correlation methods to align a large number of images for averaging. The averaging of the aligned images leads to the enhancement of structure that is shared by the images and in this way increases the signal to noise ratio. For this method to be useful, the images must be similar. Separation of different structural arrangements by the application of hierarchical classification methods (Frank et al., 1982; Bretaudiere and Frank, 1986) has been partially successful (Owen, Frank, Weisel, and Pepe, unpublished results). However, a cleaner separation into groups of similar images is obtained from examination of images after imposing threefold symmetry by rotational averaging of the individual images (Fig. 2). The observed different patterns must result from structures with different arrangements of subfilaments. After having separated the images into groups with similar structure, the symmetry of the structure in each group can be determined in an unbiased way. Cross-correlation alignment and averaging of the images in each group consistently provided evidence for threefold symmetry (Fig. 3). Attempts to bias the alignment in favor of other symmetries failed (Fig. 3, *d–g*). This and the other evidence for threefold symmetry discussed above justifies the application of methods for enhancing the threefold structural symmetry of the images (as in Fig. 2).

Subfilament arrangement in transverse sections

Three arrangements of subfilaments were observed at ionic strengths of both 20 and 200 mM (Fig. 2, *a*, *b*, and *c*). Diagrammatic representations of these arrangements are shown in Fig. 10. The three arrangements were observed in all regions of the filament and for different filaments in the same section, i.e., at the same level. At an ionic strength of 200 mM a fourth arrangement was observed (Fig. 2 *d*). (This fourth arrangement was only rarely observed at 20 mM ionic strength.) It appeared to be intermediate between those in Fig. 2, *a* and *b*, suggesting a transition between them. This arrangement is shown diagrammatically in Fig. 10 *d*. The representation of each of the different arrangements from region to region along the filament did not change substantially at an ionic strength of 200 mM; but at an ionic strength of 20 mM there were differences with one arrangement predominating at the expense of the other on moving from the P to the D region of the filament. At low ionic strength, where there appears to be a change along the length of the filament from one arrangement to another, the transitional arrangement was only rarely observed, whereas at the higher ionic strength, where a particular arrangement was about equally represented in all regions of the filament, the transitional arrangement was commonly observed. It appears that the transitional arrangement may be stabilized by the higher ionic strength.

In the average images (Fig. 2) the density of the three central subfilaments often appeared higher than that of the peripheral subfilaments (Pepe et al., 1986). The individual images used to produce these averages generally did not show this kind of difference. A possible explanation for the apparent difference in subfilament densities in the averages could be that variation in position of the central subfilaments is considerably less

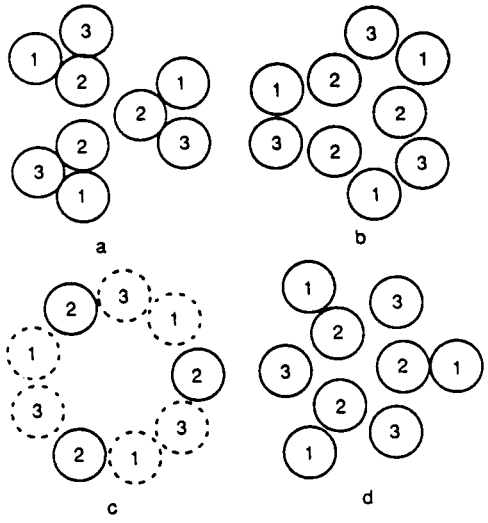

FIGURE 10 Diagrammatic representation of the different arrangements of subfilaments observed in Fig. 2. (*a*) The arrangement observed in Fig. 2 *b*. (*b*) The arrangement observed in Fig. 2 *a*. (*c*) The arrangement observed in Fig. 2 *c*. In this average image only three densities are seen clearly with additional less dense material present between them at the surface of the filament. The clearly observed densities correspond to the three subfilaments in individual images which superimposed closely. The other six subfilaments observed in the individual images had more variable positions (as indicated by dashed circles) and therefore were not enhanced in the average image in Fig. 2 *c*. (*d*) In this arrangement with three central subfilaments (Fig. 2 *d*), the surface subfilaments are in positions intermediate to those in *a* and *b*. The peaks of power as a function of radius in Fig. 5 for a frequency of 3 were used to determine the radial position of the three central subfilaments in *a* and *b*. For the arrangement in *a* (which corresponds to Fig. 2 *b*), this distance is 2.75 nm, whereas that in *b* (corresponding to Fig. 2 *a*) is 3.0 nm. The radial position of the peripheral subfilaments in *c* (corresponding to Fig. 2 *c*), is at 6.0 nm which was taken to be the same as that for the peripheral subfilaments of a pair in *a* and *b*. The spacing between the subfilaments of a pair on the surface was measured from enlargements of Fig. 2, *a* and *b*, and found to be 4.0 nm in both cases. From these measurements all the other spacings were calculated. In *a*, the spacing between the peripheral subfilaments, 3 or 1, and a central subfilament, 2, was calculated to be 3.5 nm. This was taken as the diameter of all the subfilaments and is consistent with measurements made previously on highly selected images (Pepe and Drucker, 1972). The spacing between the central subfilaments was calculated as 4.8 nm. In *b*, the spacing between the peripheral subfilaments, 3 or 1, and a central subfilament was calculated as 4.0 nm and the spacing between central subfilaments as 5.0 nm. In *c*, if all nine subfilaments had been more precisely superimposable at the 6.0-nm radial position of the three observed in Fig. 2 *c*, the spacing between all nine subfilaments would be 4.0 nm. Measurements were not made on the average image in Fig. 2 *d*, corresponding to the diagram in *d*.

than that of the peripheral subfilaments. A large enough deviation from the average position for some of the peripheral subfilaments will result in their contributing to background density without overlapping the average subfilament position thus leading to an apparent lower density for those subfilaments. In the average image in Fig. 2 *c* where all the density is on the surface, again there are three subfilaments with high density and other density which is not clearly resolved. Similarly in this case the position of three of the subfilaments matched closely among the individual images in the average leading to their intensification. The variation in position of the other six subfilaments on the surface in the individual images making up the average was large enough that they were not resolved individually in the average but contributed to the density present in between the three dense subfilaments on the surface of the filament. In Fig. 10 *c* the variability in position of six of the nine subfilaments is indicated by the dashed circles. It is tempting to speculate that the three dense surface subfilaments in Fig. 2 *c* and the central subfilaments in Fig. 2, *a* and *b*, represent displacement of the same subfilaments between the center and surface of the filament as suggested in Fig. 10.

In an attempt to determine if there was a preferential orientation or superlattice arrangement of the filaments in the A-band the relative orientations of the individual filaments was studied. The three central subfilaments of the individual images in the averages in Fig. 2, *a*, *b*, and *d*, and the three dense subfilaments in Fig. 2 *c* were used as the reference for orientation. By plotting the frequency distribution of the angles required to bring these three subfilaments in register for all the filament images obtained from the same section, it was found that there was a preference for filaments to occur with a 90° difference in orientation between them. However, there was no recognizable pattern to the occurrence of these orientation differences in the lattice. It is conceivable that these observations may have some relation to the complex superlattice described by Luther and Squire (1980) in frog muscle.

Longitudinal alignment of subfilaments

Different possibilities have been suggested for the structure of the backbone, ranging from the equivalent packing of individual myosin molecules and twisted rope models (Squire, 1973; 1981) to the parallel alignment of subfilaments made up of parallel staggered myosin molecules (Pepe, 1966*b*, 1967*a*; Pepe et al., 1986). The splaying of separated myosin filaments into three parallel units under appropriate conditions (Maw and Rowe, 1980; Pepe, 1982) provides evidence for the parallel organization of at least three structural units in the backbone of the filament but does not give information about the organization within these units. Transverse sections of the myosin filaments have also been studied to analyze the longitudinal alignment of structures in the

backbone of the filament. Optical diffraction patterns obtained from incrementally tilted images of the same transverse section showed changes in the diffraction pattern with tilt which were consistent with the presence of parallel rods (Pepe and Dowben, 1977; Pepe et al., 1981; Stewart et al., 1981).

In a single transverse section in the present work, different arrangements of subfilaments appeared to occur randomly in the myosin filament lattice. One way to reconcile different arrangements of subfilaments with parallel subfilaments would be to have classes of filaments with different packing of subfilaments in the backbone. To investigate this possibility we looked at serial sections of the same filament and found that the arrangement of subfilaments in three serial sections of the same filament are generally not all the same. If the subfilaments are not parallel but rather twist around the long axis of the filament, one would expect that superposition of the three serial sections on their three-fold centers without rotation would obscure the subfilaments. When this was done for 27 filaments in which all three serial sections had threefold symmetry, the majority (78%) of the average images had threefold symmetry in the arrangement of the subfilaments. Therefore for a total length of 330 nm along the filament the subfilament positions are similar but vary around an average position which corresponds to one of the arrangements observed. This result could be accounted for by having one of the different arrangements predominating in the average. It may be that the assembly of these different arrangements is energetically very similar, with the resulting relative proportion of the arrangements reflecting small differences in stability.

At low ionic strength (20 mM) the predominance of the arrangement in Fig. 10 *a* in the P region of the filament and that in Fig. 10, *b* or *c*, in the D region, suggests a gradual transition along the length of the filament. The transition would occur over a length of ~0.75 μm. A 4-nm shift of subfilaments 3 and 1 will result in changing from the arrangement in Fig. 10 *a* to that in Fig. 10 *b*. A shift of 4 nm over this length would result in a tilt of the subfilaments of 0.003°, which is essentially no tilt. Therefore even with a gradual transition along 0.75 μm of the filament length, the subfilaments are essentially parallel to the long axis.

There is considerable evidence suggesting that there may be structural differences along the length of the myosin filament. The restricted binding of C-protein to the C region of the filament (Offer, 1972; Craig and Offer, 1976; Pepe and Drucker, 1975) suggests that the C-protein–binding sites on myosin are only available in the C region and are blocked along the rest of the filament. The nonuniform labeling of the A-band by monoclonal and polyclonal antibodies specific for myosin (Wachsberger et al., 1983; Pepe, 1976) similarly suggests differences in the myosin packing along the length of the filament that affect the availability of epitopes for antibody binding on the surface. Although we observed differences in subfilament organization along the length of the filament at an ionic strength of 20 mM, and no differences at the higher ionic strength of 200 mM, the structural information we presently have cannot be related directly to the different availability of epitopes and other protein binding sites on the filament.

This study suggests a rather complex structure for the backbone of the myosin filament. The major findings can be summarized as follows: (*a*) The myosin subfilaments, on average remain parallel to the long axis of the filament. (*b*) Three different arrangements of subfilaments are observed at ionic strengths of both 20 and 200 mM. A fourth arrangement appearing to be intermediate between two of these is seen often at 200 mM and only rarely at 20 mM. (*c*) At low ionic strength (20 mM) there appears to be a transition along the length of the filament such that one arrangement predominates in the P region and another in the D region. Because this occurs over one-half of the length of the filament (~0.75 μm) it results in a subfilament tilt of only 0.003°. (*d*) At the higher (200 mM) ionic strength comparison of the backbone structure under rigor and relaxed conditions shows no differences in the subfilament organization.

We are grateful for the assistance of Dr. Yale Goldman and Jonathan Tanner in the preparation and handling of single skinned fibers and small bundles of skinned fibers.

This work was supported by U.S. Public Health Service grant HL-15835 to the Pennsylvania Muscle Institute and by Basic Research Support Grants 2-S0-RR-05415-28 and 2-S07-RR-0783-23 sub 27.

Received for publication 20 December 1990 and in final form 30 January 1992.

REFERENCES

Ashton, F., and F. A. Pepe. 1981. The myosin filament. VIII. Preservation of subfilament organization. *J. Microsc.* 123:93–108.

Brenner, B., L. C. Yu, and R. Podolsky. 1984. X-ray diffraction evidence for cross bridge formation in relaxed muscle fibers at various ionic strengths. *Biophys. J.* 46:299–306.

Bretaudiere, J., and J. Frank. 1986. Reconstitution of molecule images analyzed by correspondence analysis: a tool for structural interpretation. *J. Microsc.* 144:1–14.

Cantino, M., and J. M. Squire. 1986. Resting myosin crossbridge configuration in frog muscle thick filaments. *J. Cell Biol.* 102:610–618.

Craig, R., and G. Offer. 1976. The location of C-protein in rabbit skeletal muscle. *Proc. R. Soc. Lond. Ser. B.* 192:451–461.

Crowther, R., and L. Amos. 1971. Harmonic analysis of electron microscopic images with rotational symmetry. *J. Mol. Biol.* 60:123–130.

Dantzig, J. A., and Y. E. Goldman. 1985. Suppression of muscle contraction by vanadate. *J. Gen. Physiol.* 86:305–327.

Frank, J., B. Shimkin, and H. Dowse. 1981*a*. SPIDER—a modular software system for electron image processing. *Ultramicroscopy.* 6:343–358.

Frank, J., A. Verschoor, and M. Boublik. 1981*b*. Computer averaging of electron micrographs of 40S ribosomal subunits. *Science (Wash. DC).* 214:1353–1355.

Frank, J., A. Verschoor, and M. Boublik. 1982. Multivariate statistical analysis of ribosome electron micrographs: L and R lateral views of the 40 S subunit from HeLa cells. *J. Mol. Biol.* 161:107–137.

Hanada, K., M. Tamai, S. Morimoto, T. Adachi, S. Ohmura, J. Sawada, and I. Tanaka. 1978. Inhibitory activities of E 64 derivatives of papain. *Agric. Biol. Chem.* 42:537–541.

Huxley, E. H. 1963. Electron microscopic studies on the structure of natural and synthetic protein filaments from striated muscle. *J. Mol. Biol.* 7:281–308.

Huxley, H. E., and W. Brown. 1967. The low-angle X-ray diagram of vertebrate striated muscle and its behavior during contraction and rigor. *J. Mol. Biol.* 30:383–434.

Ip, W., and J. Heuser. 1983. Direct visualization of the myosin crossbridge lattice on relaxed rabbit psoas thick filaments. *J. Mol. Biol.* 171:105–109.

Kensler, R., and M. Stewart. 1983. Frog skeletal muscle thick filaments are three stranded. *J. Cell Biol.* 96:1797–1802.

Kensler, R., and M. Stewart. 1986. An ultrastructural study of cross-bridge arrangement in the frog thigh muscle thick filament. *Biophys. J.* 49:343–351.

Knight, P. J., M. A. Erickson, M. E. Rodgers, M. Beer, and J. W. Wiggins. 1986. Distribution of mass within native thick filaments of vertebrate skeletal muscle. *J. Mol. Biol.* 189:167–177.

Luther, P. K., and J. M. Squire. 1980. Three-dimensional structure of the vertebrate muscle A-band II: the myosin filament superlattice. *J. Mol. Biol.* 141:409–439.

Luther, P. K., P. M. G. Munro, and J. M. Squire. 1981. Three-dimensional structure of the vertebrate muscle A-band III: M-region and myosin filament symmetry. *J. Mol. Biol.* 151:703–730.

Maw, M. C., and A. J. Rowe. 1980. Fraying of A-filaments into three subfilaments. *Nature (Lond.).* 286:412–440.

Millman, B. 1979. X-ray diffraction from chicken skeletal muscle. *In* Motility in Cell Function. F. A. Pepe, J. W. Sanger, and V. T. Nachmias, editors. Academic Press, Inc., New York. 351–354.

Offer, G. 1972. C-protein and the periodicity in the thick filaments of vertebrate skeletal muscle. *Cold Spring Harbor Symp. Quant. Biol.* 37:87–93.

Pepe, F. A. 1966*a*. Some aspects of the structural organization of the myofibril as revealed by antibody-staining methods. *J. Cell Biol.* 28:505–525.

Pepe, F. A. 1966*b*. Organization of myosin molecules in the thick filament of striated muscle as revealed by antibody staining in electron microscopy. *Electron Microsc.* 2:53–54.

Pepe, F. A. 1967*a*. The myosin filament. I. Structural organization from antibody staining observed in electron microscopy. *J. Mol. Biol.* 27:203–225.

Pepe, F. A. 1967*b*. The myosin filament. II. Interaction between myosin and actin filament observed using antibody staining in fluorescent and electron microscopy. *J. Mol. Biol.* 27:227–236.

Pepe, F. A. 1971. The structure of the myosin filament of striated muscle. *Prog. Biophys. Mol. Biol.* 22:77–96.

Pepe, F. A. 1976. Detectability of antibody in fluorescence and electron microscopy. *In* Cell Motility. *Cold Spring Harbor Conf. Cell Proliferation.* 3:337–346.

Pepe, F. A. 1982. The structure of vertebrate skeletal muscle myosin filaments. *In Cell Muscle Motil.* 2:141–171.

Pepe, F. A., F. T. Ashton, P. Dowben, and M. Stewart. 1981. The myosin filament. VII. Changes in internal structure along the length of the filament. *J. Mol. Biol.* 145:421–440.

Pepe, F. A., F. T. Ashton, C. Street, and J. Weisel. 1986. The myosin filament. X. Observation of nine subfilaments in transverse sections. *Tissue Cell.* 18:499–508.

Pepe, F. A., and P. Dowben. 1977. The myosin filament. V. Intermediate voltage electron microscopy and optical diffraction studies of the substructure. *J. Mol. Biol.* 113:199–218.

Pepe, F. A., and B. Drucker. 1972. The myosin filament. IV. Observations of the internal structural arrangement. *J. Cell. Biol.* 52:225–260.

Pepe, F. A., and B. Drucker. 1975. The myosin filament. III. C-protein. *J. Mol. Biol.* 99:609–617.

Sachs, L. 1984. Applied Statistics: A Handbook of Techniques. 2nd edition. Springer-Verlag, Inc., New York.

Sjostrom, M., and J. M. Squire. 1977. Fine structure of the A-band in cryo-sections: the structure of the A-band of human skeletal muscle fibers from ultra-thin cryo-sections negatively stained. *J. Mol. Biol.* 109:49–68.

Squire, J. M. 1973. General model of myosin filament structure. III. Molecular packing arrangement in myosin filaments. *J. Mol. Biol.* 77:291–323.

Squire, J. M. 1981. The Structural Basis of Muscle Contraction. Plenum Publishing Corp., New York.

Stewart, M., F. T. Ashton, R. Liberson, and F. A. Pepe. 1981. The myosin filament. IX. Determination of subfilament positions by computer processing of electron micrographs. *J. Mol. Biol.* 153:381–392.

Stewart, M., and R. W. Kensler. 1986. Arrangement of myosin heads in relaxed thick filaments from frog skeletal muscle. *J. Mol. Biol.* 192:831–851.

Van Heel, M. 1987. Similarity measure between images. *Ultramicroscopy.* 21:95–100.

Varrano-Marston, E., C. Franzini-Armstrong, and J. C. Haselgrove. 1984. The structure and disposition of cross bridges on deep-etched fish muscle. *J. Muscle Res. Cell Motil.* 5:363–383.

Wachsberger, P., L. Lampson, and F. A. Pepe. 1983. Nonuniform staining of myofibril A-bands by a monoclonal antibody to skeletal muscle myosin S1 heavy chain. *Tissue Cell.* 15:341–350.

Wray, J. 1979. Structure of the backbone in myosin filaments of muscle. *Nature (Lond.).* 270:37–40.

Zingsheim, H. P., F. J. Barrantes, J. Frank, W. Hanicke, and D.-C. Neugebauer. 1982. Direct structural localization of two toxin-recognition sites on an A Ch receptor protein. *Nature (Lond.).* 299:81–84.